BIOLOGY, MEDICINE, & NATURAL PRODUCT CHEMISTRY ISSN 2089-6514 (paper)
Volume 15, Number 2, October 2026 | Pages: 2071-2079 | DOI: 10.14421/biomedich.2026.152.2071-2079 ISSN 2540-9328 (online)

Predominantly Amorphous Atorvastatin Calcium–Nicotinamide Solid: Solid-State Characterisation and Dissolution Enhancement

Indra Indra*, Wida Salsabila Diena, Ade Yeni Aprillia, Winda Trisna Wulandari
Department of Pharmaceutics, Faculty of Pharmacy, Universitas Bakti Tunas Husada,
Jl. Letjen Mashudi No. 20, Tasikmalaya 46196, Indonesia. Tel: +62-265-334740.

Corresponding author*
indra@universitas-bth.ac.id

Manuscript received: 21 June 2026. Revision accepted: 04 November 2026, Published: 09 November 2026.

Abstract

Atorvastatin calcium is a poorly water-soluble drug whose oral performance is limited by low aqueous solubility and slow dissolution. This study prepared an atorvastatin calcium–nicotinamide multicomponent solid by solvent evaporation and classified its solid-state form using integrated physicochemical characterisation. Atorvastatin calcium and nicotinamide were processed at a 1:1 molar ratio using an ethanol–acetone solvent system. The parent compounds, physical mixture, and solvent-evaporated solid were evaluated using powder X-ray diffraction, Fourier transform infrared spectroscopy, differential scanning calorimetry, thermogravimetric analysis, and scanning electron microscopy. Aqueous solubility and dissolution performance were also assessed. The processed atorvastatin calcium–nicotinamide solid showed a broad diffuse halo with marked attenuation of the characteristic crystalline peaks of both parent compounds, supporting reduced long-range crystallographic order rather than formation of a well-defined crystalline cocrystal. Spectral changes in the O–H/N–H and carbonyl/amide regions supported intermolecular interaction, while thermal and morphological analyses further indicated solid-state transformation. The transformed solid increased aqueous solubility from 1.41 ± 0.02 to 5.61 ± 0.04 mg/mL and produced faster dissolution than crystalline atorvastatin calcium in both 0.1 N HCl and phosphate buffer media. Overall, the data support formation of a predominantly amorphous or co-amorphous atorvastatin calcium–nicotinamide multicomponent solid with possible residual crystallinity. The improved apparent solubility and dissolution are plausibly associated with reduced crystallinity and atorvastatin calcium–nicotinamide intermolecular interaction.

Keywords: Amorphous multicomponent solid; Atorvastatin calcium; Dissolution enhancement; Nicotinamide; Solid-state characterization.

Abbreviations: ATC, atorvastatin calcium; DSC, differential scanning calorimetry; FTIR, Fourier transform infrared spectroscopy; NIC, nicotinamide; PM, physical mixture; PXRD, powder X-ray diffraction; SEM, scanning electron microscopy; TGA, thermogravimetric analysis.

INTRODUCTION

Poor aqueous solubility remains a major limitation in the oral formulation of many active pharmaceutical ingredients, particularly those classified as Biopharmaceutics Classification System (BCS) class II drugs. For these compounds, intestinal permeability is generally adequate, but dissolution in gastrointestinal fluids becomes a rate-limiting step for absorption and systemic exposure. Atorvastatin calcium (ATC), a widely used HMG-CoA reductase inhibitor, is a representative BCS class II drug with low aqueous solubility, limited and variable oral bioavailability, and pH-dependent dissolution behaviour (Al-Kazemi et al., 2019; Telange et al., 2023). Consequently, improving its apparent solubility and dissolution rate remains an important formulation objective.

Solid-state modification has been widely investigated as a strategy to improve the biopharmaceutical performance of poorly water-soluble drugs without altering their covalent structure. Approaches such as polymorph control, amorphisation, solid dispersion, cocrystallisation, and co-amorphous formulation can modify crystal packing, intermolecular interactions, surface properties, and thermodynamic activity, thereby influencing solubility and dissolution behaviour (Gadade & Pekamwar, 2016; Karagianni et al., 2018). Among these approaches, pharmaceutical cocrystals and co-amorphous systems are particularly attractive because they employ low-molecular-weight coformers to alter the drug's solid-state arrangement via noncovalent interactions, primarily hydrogen bonding, while preserving the chemical identity of the active compound.

Nicotinamide has frequently been selected as a pharmaceutical coformer because it contains complementary hydrogen-bond donor and acceptor sites and participates in supramolecular interactions with poorly soluble drugs. Previous studies have reported

atorvastatin calcium–nicotinamide multicomponent solids prepared by solvent evaporation or solvent-assisted grinding, with improvements in solubility and dissolution compared with untreated ATC (Shayanfar & Jouyban, 2014). Shayanfar et al. (2013) described an ATC–nicotinamide co-amorphous system prepared by solvent evaporation, whereas Al-Kazemi et al. (2019) reported ATC cocrystals with nicotinamide and glucosamine using different drug–coformer ratios and preparation methods. These studies indicate that nicotinamide is a relevant coformer for ATC solid-state modification.

However, the solid-form assignment of ATC–nicotinamide systems remains scientifically challenging. A critical commentary by Emami and Shayanfar (2020) questioned the adequacy of evidence for cocrystal formation in some ATC cocrystallisation studies, particularly when DSC thermograms do not show a single distinct melting event and when solid residues after solubility testing are not characterised. They also noted that solvent evaporation itself may transform ATC into a semi-crystalline or less crystalline form, meaning that a changed PXRD pattern cannot automatically be attributed to cocrystal formation. This concern is especially relevant for ATC, whose hydrate state, dehydration behaviour, and crystallinity can be affected by processing conditions (Akour et al., 2025; Skotnicki et al., 2021).

Accurate classification of pharmaceutical multicomponent solids, therefore, requires an integrated analytical approach. PXRD is essential for distinguishing new crystalline phases from amorphous halo patterns or physical mixtures; FTIR provides evidence of hydrogen-bonding changes but cannot independently confirm solid-form identity; DSC supports phase-transition interpretation but may not distinguish cocrystals, eutectics, and amorphous systems without orthogonal evidence; TGA assists in evaluating water or solvent loss; and SEM provides supportive morphological information rather than definitive structural proof (Saganowska & Wesolowski, 2017; Wesolowski, 2025). Such integration is particularly important when the final product shows reduced crystallinity rather than sharp new Bragg reflections.

The present study addresses this need by preparing an ATC–nicotinamide multicomponent solid using solvent evaporation and evaluating its solid-state transformation and pharmaceutical performance using PXRD, FTIR, DSC, TGA, SEM, solubility testing, and dissolution studies. The novelty of this work lies not in claiming the formation of a new crystalline cocrystal, but in applying a cautious, multi-technique interpretation framework to classify the ATC–nicotinamide solid and relate its solid-state features to solubility and dissolution enhancement. This study specifically investigated whether solvent evaporation of ATC with nicotinamide produces a crystalline cocrystal, a co-amorphous/amorphous multicomponent solid, or another solid-state form, and how this transformation influences aqueous solubility and dissolution behaviour.

MATERIALS AND METHODS

Materials

Atorvastatin calcium (ATC) and nicotinamide (NIC) were obtained from PT Kimia Farma (Bandung, Indonesia). Ethanol and acetone were purchased from Merck (Darmstadt, Germany). Distilled water, 0.1 N HCl (pH 1.2), and phosphate buffer (pH 6.8) were used as solubility and dissolution media. All chemicals and solvents were of analytical grade and used without further purification.

Preparation of ATC–NIC Multicomponent Solid and Physical Mixture

The ATC–NIC multicomponent solid was prepared by solvent evaporation. ATC and NIC were weighed at a 1:1 molar ratio, corresponding to 100 mg ATC and 10.1 mg NIC, and dissolved in 2 mL ethanol–acetone mixture (2:8, v/v). The solution was stirred magnetically at room temperature until clear, then covered with perforated parafilm to allow slow evaporation under ambient conditions. Evaporation was continued for approximately 2–3 days until a dry solid was obtained. The product was stored in a desiccator for 24 h before characterisation and testing. No sieving was performed before analysis.

The physical mixture (PM) was prepared by manually blending ATC and NIC at a 1:1 molar ratio in a mortar and pestle until visually homogeneous. The PM was not sieved and was used only as a solid-state characterisation control; it was not subjected to solubility or dissolution testing.

Powder X-ray Diffraction

PXRD patterns of ATC, NIC, PM, and ATC–NIC were recorded using a Shimadzu XRD-7000 diffractometer (Shimadzu Corporation, Kyoto, Japan) with CuKα radiation (λ = 1.5406 Å). The instrument was operated at 40 kV and 30 mA. Samples were scanned over 3–40° 2θ using a step size of 0.02° and a scan speed of 2°/min. Powder samples were placed directly on the sample holder without further pretreatment. Diffraction profiles were compared based on characteristic reflections, peak attenuation or disappearance, peak broadening, and diffuse halo formation.

Fourier Transform Infrared Spectroscopy

ATR-FTIR spectra of ATC, NIC, PM, and ATC–NIC were collected using an Agilent Cary 630 FTIR spectrometer (Agilent Technologies, Santa Clara, CA, USA). Spectra were recorded from 4000 to 650 cm^{-1} at a resolution of 4 cm^{-1} with 32 scans per spectrum. Powder samples were placed directly on the ATR crystal, and spectra were acquired after adequate sample–crystal

contact. Spectral comparison focused on O–H/N–H stretching, carbonyl/amide vibrations, carboxylate-related bands, aromatic vibrations, and C–N stretching regions.

Differential Scanning Calorimetry

DSC analysis of ATC, NIC, PM, and ATC–NIC was performed using a Shimadzu DSC-60 Plus differential scanning calorimeter (Shimadzu Corporation, Kyoto, Japan). Approximately 3 mg of each sample was placed in crimped aluminium pans with pierced lids. Samples were heated from 30 to 200 °C at 10 °C/min under a nitrogen flow rate of 50 mL/min. Thermal events were identified from the recorded heat-flow profiles.

Thermogravimetric Analysis

TGA was used to evaluate the mass-loss behaviour of ATC, NIC, PM, and ATC–NIC. Approximately 3–5 mg of each sample was placed in an alumina pan and heated from 30 to 400 °C at 10 °C/minutes under nitrogen flow at 50 mL/minutes using a Shimadzu TGA-50/DTG-60H thermogravimetric analyser (Shimadzu Corporation, Kyoto, Japan). Weight-loss profiles were examined for low-temperature mass loss attributable to water or residual solvent, and for subsequent thermal decomposition.

Scanning Electron Microscopy

The morphology of ATC and ATC–NIC was examined using a JEOL JSM-6510LA scanning electron microscope (JEOL Ltd., Tokyo, Japan). Powder samples were mounted on aluminium stubs with double-sided carbon adhesive tape and sputter-coated with gold or gold–palladium before observation. Micrographs were obtained at an accelerating voltage of 10–15 kV under high vacuum. Morphological comparison focused on particle habit, surface texture, aggregation, and particle-boundary definition.

Saturation Solubility Study

Saturation solubility was determined for ATC and ATC–NIC in distilled water. An excess amount of each sample, corresponding to 30 mg of solid, was added to 10 mL of distilled water. Suspensions were stirred at 300 rpm and maintained at 37 °C for 24 hours. After equilibration, samples were filtered through a 0.45 µm membrane filter without centrifugation. The filtrates were analysed at 246 nm using a GENESYS 50 UV–Visible spectrophotometer (Thermo Fisher Scientific, Waltham, MA, USA). Solubility was expressed as mg/mL of ATC. Measurements were performed in triplicate and reported as mean ± standard deviation.

In Vitro Dissolution Study

The dissolution behaviour of ATC and ATC–NIC was evaluated using the USP apparatus II paddle method with a BIOBASE dissolution tester (BIOBASE Group, Jinan, China). Dissolution was performed in 900 mL of 0.1 N HCl (pH 1.2) and phosphate buffer (pH 6.8) at 37 ± 0.5 °C and 100 rpm. Each test used a sample equivalent to 300 mg ATC. Aliquots were withdrawn at 5, 10, 15, 30, 45, and 60 min and immediately replaced with an equal volume of fresh medium maintained at the same temperature. Samples were filtered through a 0.45 µm membrane filter and analysed at 246 nm using a GENESYS 50 UV–Visible spectrophotometer. Volume replacement and dilution corrections were applied. Dissolution experiments were performed in triplicate, and results were expressed as a percentage of ATC dissolved over time.

Data Analysis

Experimental data were processed using Microsoft Excel. Solubility and dissolution results from three independent replicates were presented as mean ± standard deviation. No inferential statistical analysis was applied. PXRD, FTIR, DSC, and TGA profiles were plotted from the raw data without smoothing. Diffraction peaks, spectral bands, and thermal events were manually assigned through direct comparison among ATC, NIC, PM, and ATC–NIC. Solid-state classification was based on the integrated interpretation of PXRD, FTIR, DSC, TGA, and SEM data, whereas solubility and dissolution data were used to evaluate pharmaceutical performance.

RESULTS AND DISCUSSION

Preparation of ATC–NIC Multicomponent Solid

ATC–NIC was prepared by solvent evaporation at a 1:1 molar ratio to promote molecular association between atorvastatin calcium (ATC) and nicotinamide (NIC). The selection of NIC was based on its amide N–H and carbonyl groups, which can complement the hydroxyl, carbonyl, and carboxylate functionalities of ATC. This functional-group complementarity provided the rationale for forming a multicomponent solid, but the product's solid-state identity was not inferred from the preparation alone.

The solvent-evaporated product was obtained as a dry solid and denoted as ATC–NIC. A 1:1 physical mixture was prepared separately as ATC–NIC PM to distinguish processing-induced solid-state transformation from simple component blending. This control is essential because a physical mixture is expected to retain the crystallographic, thermal, and vibrational features of the parent compounds. Previous atorvastatin–nicotinamide systems have been classified as either cocrystalline or co-amorphous, depending on the preparation conditions and interpretation criteria (Fo'ad et al., 2022; Ghyadh & Al-Khedairy, 2023). Therefore, the present ATC–NIC solid was classified using integrated PXRD, FTIR, DSC, TGA, and SEM evidence.

PXRD Evidence of Amorphisation and Solid-State Transformation

PXRD was used as the primary technique to assess crystallographic order and distinguish ATC–NIC from the physical mixture (Figure 1). Pure ATC showed characteristic reflections at approximately 9.01°, 10.11°, 16.88°, 19.29°, 21.45°, 22.50°, and 23.12° 2θ, consistent with its crystalline or semicrystalline character. NIC displayed sharper reflections, particularly at approximately 14.81°, 22.23°, 25.68°, 27.27°, and 36.97° 2θ, confirming its crystalline nature.

The ATC–NIC PM retained the main reflections of both parent compounds. NIC peaks at approximately 14.79°, 25.75°, and 36.99° 2θ remained visible, while ATC-related reflections at approximately 16.84°, 19.25°, 21.41°, 22.38°, and 23.12° 2θ were also preserved. This superimposed pattern indicates that manual blending did not substantially disrupt the crystal lattices of either component.

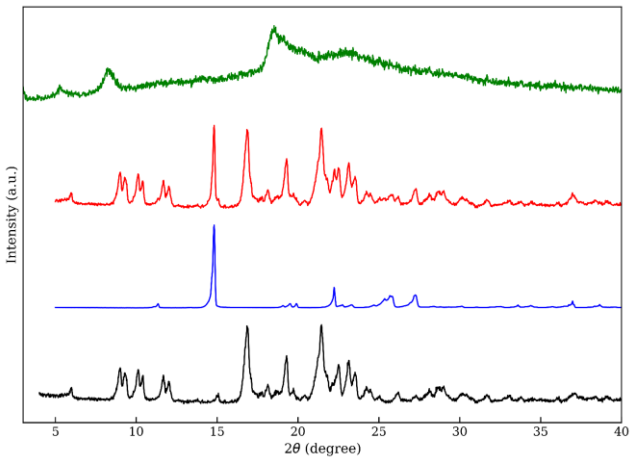


Figure 1. PXRD patterns of atorvastatin calcium (ATC), nicotinamide (NIC), physical mixture (PM), and solvent-evaporated ATC–NIC multicomponent solid.

The solvent-evaporated ATC–NIC solid showed a distinctly different PXRD profile. The sharp reflections of ATC and NIC were largely attenuated, and the diffractogram was dominated by a broad diffuse halo centred around 18–23° 2θ. The disappearance of the intense NIC reflections and the loss of several ATC crystalline peaks indicate a marked reduction in long-range crystallographic order. No new set of sharp Bragg reflections was observed; therefore, the PXRD data do not support the formation of a well-defined crystalline cocrystal (Dutt et al., 2021; Ouiyangkul et al., 2020). Instead, the profile is more consistent with predominant amorphisation or formation of an amorphous/co-amorphous multicomponent solid with possible residual crystallinity.

This interpretation aligns with accepted solid-form classification criteria. Physical mixtures generally retain the combined diffraction peaks of the starting materials, whereas crystalline cocrystals show new sharp reflections absent from the parent compounds. In contrast, amorphous and co-amorphous solids are characterised by attenuation or disappearance of Bragg peaks and the appearance of diffuse halo patterns (Haskins & Zaworotko, 2021; Indra et al., 2025; Liu et al., 2021). The present PXRD evidence, therefore, argues against simple physical mixing and against a highly crystalline cocrystal assignment.

FTIR Evidence of Hydrogen-Bond Formation

FTIR analysis was used to evaluate whether the PXRD-observed transformation was accompanied by changes in the molecular environment of ATC and NIC (Figure 2; Table 1). The most diagnostic regions were the O–H/N–H stretching region and the carbonyl/amide region, where hydrogen-bonding interactions are expected to alter band position and shape.

Table 1. Main FTIR bands of ATC, NIC, ATC–NIC PM, and ATC–NIC.

Spectral region	ATC (cm^{-1})	NIC (cm^{-1})	ATC–NIC PM (cm^{-1})	ATC–NIC (cm^{-1})	Interpretation
O–H/N–H stretching	3362.06; 3231.60	3352.74; 3145.87	3358.3; 3149.6	3272.60	Broadening/merging of donor bands; involvement of ATC O–H and/or NIC N–H in hydrogen bonding
C=O / amide I	1649.35	1669.85	1651.2	1647.48	Downshift of NIC carbonyl contribution; C=O acts as a hydrogen-bond acceptor
Amide/ring vibration	1576.66	1599.03	1580.4	1591.57	Altered amide/pyridine environment of NIC
Aromatic/amide vibration	1513.30	1485.34	—	1531.94	Spectral reorganisation in the aromatic/amide region
Carboxylate/C–N/fingerprint	1427.57; 1312.02	1388.43; 1334.39	1390.3; 1313.9	1429.43; 1313.89	Retention of ATC-related bands with a modified local environment
Fingerprint bands	1215.11; 1155.48; 1060.43; 840.52; 743.60; 695.15	1196.48; 1151.75; 1021.29; 821.88; 775.29; 698.88	1213.2; 1155.5	1220.70; 1153.61; 1026.88; 842.38; 745.47; 691.42	Non-additive spectral changes, indicating a transformed solid state

Pure ATC exhibited broad O–H stretching bands at 3362.06 and 3231.60 cm^{-1}, while NIC showed N–H stretching bands at 3352.74 and 3145.87 cm^{-1}. In ATC–NIC PM, these bands were largely retained at 3358.3 and 3149.6 cm^{-1}, reflecting the additive spectral contribution of the parent compounds. In contrast, the processed ATC–NIC solid showed a broad band centred at 3272.60 cm^{-1}, accompanied by loss of the distinct free N–H feature of NIC. This broadening and red shift support a modified hydrogen-bonding environment involving ATC and NIC donor groups.

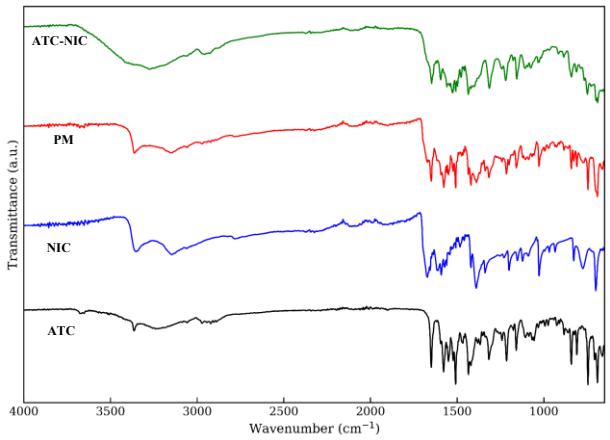


Figure 2. ATR-FTIR spectra of atorvastatin calcium (ATC), nicotinamide (NIC), physical mixture (PM), and solvent-evaporated ATC–NIC multicomponent solid.

The carbonyl/amide region further supports drug–coformer interaction. NIC showed an amide C=O band at 1669.85 cm^{-1}, while the main carbonyl-related band in ATC–NIC appeared at 1647.48 cm^{-1}. This downshift is consistent with participation of the carbonyl group as a hydrogen-bond acceptor. The NIC amide/ring vibration also shifted from 1599.03 to 1591.57 cm^{-1} in ATC–NIC, suggesting a modified local environment around the nicotinamide amide and pyridine moieties (Aljohani et al., 2017; Ghosh et al., 2021).

These changes were not reproduced by the physical mixture, supporting interaction generated during solvent evaporation rather than simple component contact. Possible interaction motifs include O–H(ATC)···O=C(NIC) and N–H(NIC)···O=C/COO^-(ATC), although these assignments remain inferential in the absence of structural confirmation. FTIR, therefore, supports molecular interaction and altered hydrogen bonding, but it cannot independently distinguish a cocrystal, co-amorphous system, or amorphous molecular dispersion. Given the PXRD halo pattern, the FTIR data are most consistent with a hydrogen-bond-associated amorphous or co-amorphous ATC–NIC solid rather than a crystalline cocrystal.

DSC Thermal Behaviour

DSC was used to examine whether the transformed ATC–NIC solid retained parent thermal events or developed a new thermal profile (Figure 3). Pure NIC exhibited a sharp endothermic event at approximately 124.10 °C. In ATC–NIC PM, a comparable event remained visible at approximately 122.1 °C, indicating that NIC largely retained its crystalline identity in the physical mixture.

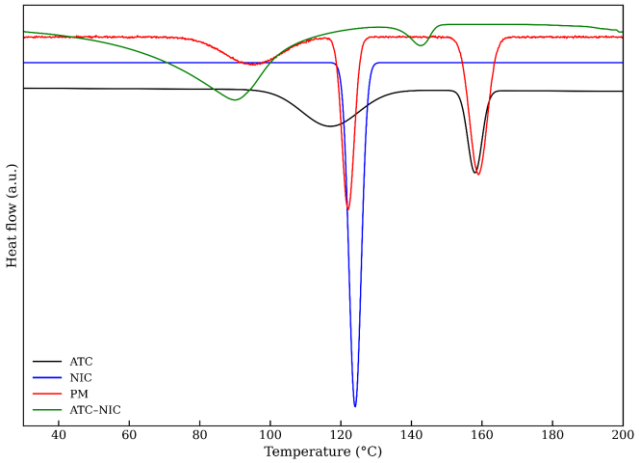


Figure 3. DSC thermograms of atorvastatin calcium (ATC), nicotinamide (NIC), physical mixture (PM), and solvent-evaporated ATC–NIC multicomponent solid.

The solvent-evaporated ATC–NIC product no longer showed the characteristic sharp NIC melting endotherm. Instead, the thermogram showed broad, complex events, including an endothermic event at 89.41 °C, a weak transition at 141.59 °C, and a broad event at 226.03 °C. The disappearance of the NIC melting endotherm supports incorporation of NIC into a transformed solid phase rather than persistence as a separate crystalline component.

The absence of a single sharp new melting endotherm also argues against assigning the product as a pure crystalline cocrystal. A crystalline cocrystal would typically show both a unique PXRD pattern with sharp reflections and a distinct melting event different from those of the parent compounds. The DSC profile observed here is more consistent with molecular disorder, amorphisation, and possible relaxation or decomposition processes within a hydrogen-bond-associated amorphous matrix (Fael & Demirel, 2020; Song et al., 2024). Because a clear glass transition was not confidently identified, the term "co-amorphous" should be used with caution. The DSC results support, but do not independently prove, the formation of a predominantly amorphous or co-amorphous ATC–NIC multicomponent solid.

TGA Analysis

TGA was performed to compare the mass-loss behaviour of ATC, NIC, ATC–NIC PM, and ATC–NIC (Figure 4). Pure ATC showed an initial mass loss of approximately

4.58% between 30 and 150 °C, attributable to adsorbed moisture and/or hydrate-associated water. Its main degradation occurred above 250 °C, with a mass loss of 43.36% between 250 and 350 °C and a residue of 40.64% at 400 °C. NIC remained relatively stable up to approximately 150 °C, followed by a major mass loss of 89.49% between 150 and 250 °C, leaving 2.00% residue at 400 °C.

The ATC–NIC PM displayed a combined thermal profile with a small low-temperature mass loss, followed by a major loss of 49.72% between 150 and 250 °C, and a further loss of 25.75% between 250 and 350 °C. The residue at 400 °C was 21.32%. This stepwise pattern reflects the contribution of both parent components and supports the physical-mixture character of PM.

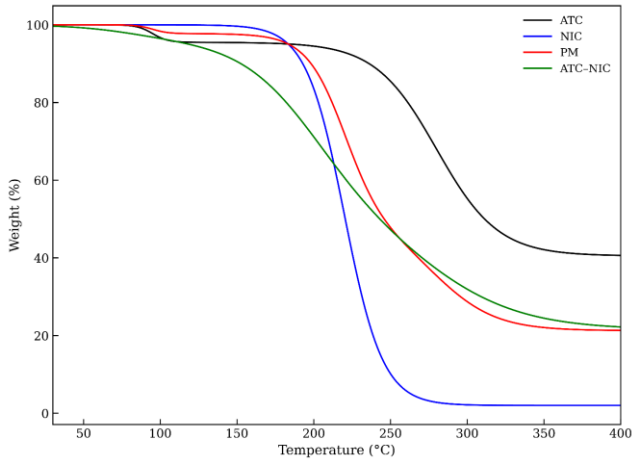


Figure 4. TGA thermograms of atorvastatin calcium (ATC), nicotinamide (NIC), physical mixture (PM), and solvent-evaporated ATC–NIC multicomponent solid.

The processed ATC–NIC solid exhibited a more gradual, continuous mass-loss profile. Its mass loss below 150 °C increased to 9.12%, suggesting greater water or residual volatile loss than in the physical mixture. The major mass loss between 150 and 250 °C was 43.31%, followed by 22.77% loss between 250 and 350 °C. The final residue at 400 °C was 22.20%, close to that of PM, indicating comparable overall residual mass but altered thermal behaviour (Gao & Zhang, 2020; Kumar et al., 2020).

The derivative trend further differentiated ATC–NIC from crystalline NIC. NIC showed a dominant mass-loss event around 220 °C, whereas ATC–NIC showed its main mass-loss rate at approximately 205.56 °C. This shift suggests that NIC did not behave as an independent crystalline phase in the processed solid. TGA therefore supports a change in thermal mass-loss pathway after solvent evaporation, although this should be interpreted as supportive evidence only. Structural classification remains primarily dependent on PXRD, FTIR, and DSC.

SEM Morphology and Particle Habit Transformation

SEM was used to assess whether the solid-state transformation was accompanied by changes in particle habit (Figure 5). Pure ATC showed elongated plate-like and needle-like particles with sharp edges, flat facets, and clear particle boundaries. This morphology is consistent with the crystalline or semicrystalline features observed by PXRD.

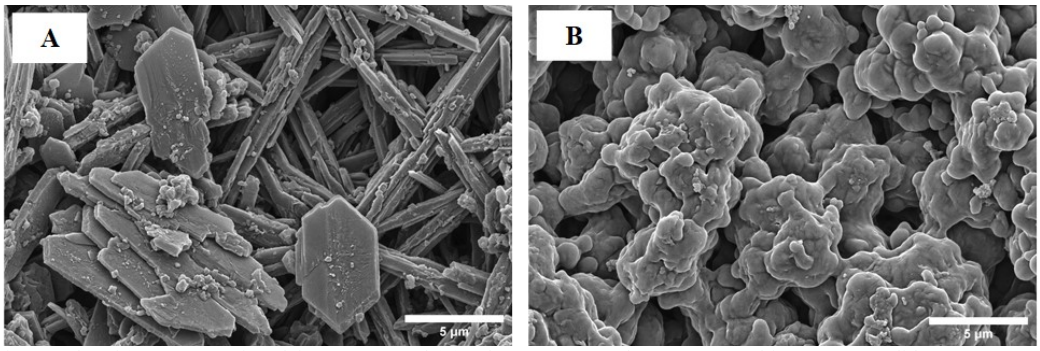


Figure 5. SEM micrographs of (A) atorvastatin calcium (ATC) and (B) solvent-evaporated ATC–NIC multicomponent solid.

The processed ATC–NIC solid exhibited a markedly different morphology. The faceted ATC particles were replaced by irregular, fused, and rounded agglomerates with less distinct particle boundaries. The surface appeared rougher and more compact, with coalesced domains forming larger secondary aggregates. This morphological change supports the disruption of the original ATC particle habit during solvent evaporation.

SEM provides complementary morphological evidence but cannot independently confirm amorphisation, co-amorphous formation, or cocrystallisation (Indra et al., 2023). The observed transition from faceted ATC crystals to irregular ATC–NIC agglomerates is consistent with the PXRD and DSC evidence for reduced crystallographic order, but the final solid-form assignment must remain based on integrated characterisation rather than morphology alone.

Solubility and Dissolution Performance

The pharmaceutical impact of ATC–NIC transformation was evaluated using aqueous solubility and dissolution

testing (Figures 6 and 7). Pure ATC showed an aqueous solubility of 1.41 ± 0.02 mg/mL, while ATC–NIC reached 5.61 ± 0.04 mg/mL, corresponding to a 3.98-fold increase. This enhancement is consistent with the reduced crystallinity and altered molecular environment observed by PXRD, FTIR, and DSC.

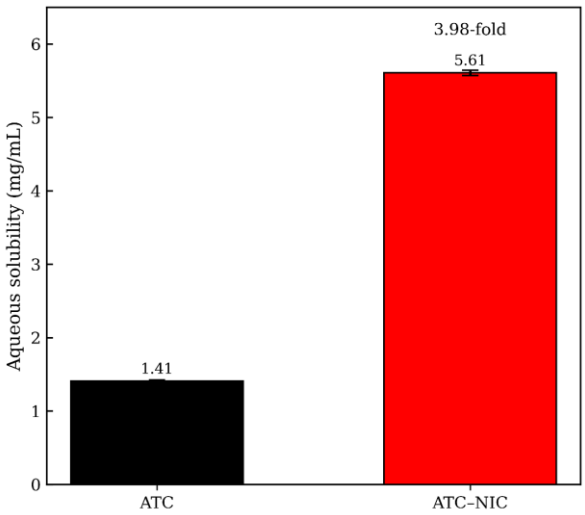


Figure 6. Aqueous solubility of atorvastatin calcium (ATC) and solvent-evaporated ATC–NIC multicomponent solid in distilled water. Data are presented as mean ± SD (n = 3).

Dissolution testing showed that ATC–NIC improved both the rate and extent of ATC release in acidic and phosphate buffer media. In 0.1 N HCl medium (pH 1.2), pure ATC released 12.00 ± 0.20% at 5 min and 62.03 ± 0.75% at 60 min. ATC–NIC released 35.00 ± 0.40% at 5 min, 87.97 ± 1.05% at 15 min, and 95.03 ± 1.05% at 60 min. The early release was therefore approximately 2.9-fold higher than pure ATC at 5 min.

A similar improvement was observed in phosphate buffer medium (pH 6.8). Pure ATC released 8.00 ± 0.10% at 5 min and 58.03 ± 0.85% at 60 min, whereas ATC–NIC released 30.00 ± 0.40% at 5 min and 96.53 ± 1.05% at 60 min. Dissolution efficiency at 60 min increased from 40.94% to 81.51% in pH 1.2 and from 37.61% to 80.83% in pH 6.8. These values show that ATC–NIC improved the overall dissolution process rather than only increasing the final dissolved fraction.

The kinetic advantage was also reflected in the estimated time to reach 50% and 80% release. Pure ATC required approximately 37.48 min to reach 50% release in pH 1.2 and 41.94 min in pH 6.8, and it did not reach 80% release within 60 min in either medium. ATC–NIC reached 50% release within 7.50 min in pH 1.2 and 8.57 min in pH 6.8, and reached 80% release within 13.27 and 14.58 min, respectively. These changes indicate faster, more complete ATC release from the processed multicomponent solid.

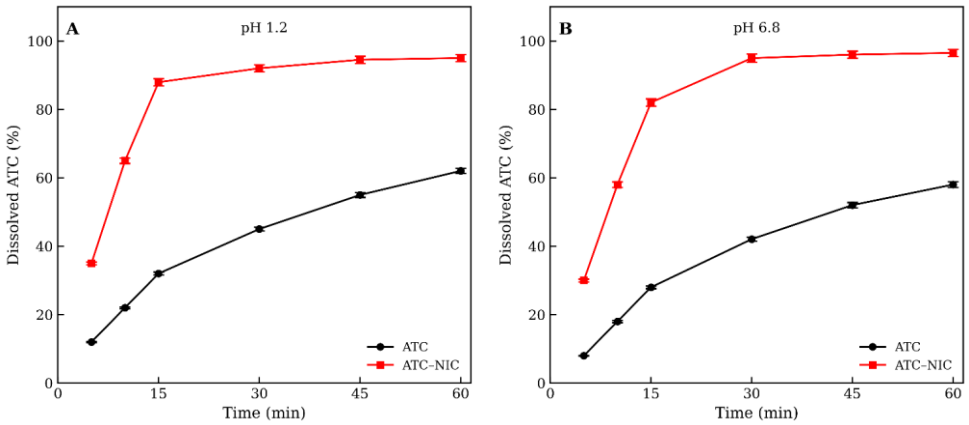


Figure 7. Dissolution profiles of atorvastatin calcium (ATC) and solvent-evaporated ATC–NIC multicomponent solid in (A) 0.1 N HCl medium, pH 1.2, and (B) phosphate buffer medium, pH 6.8. Data are presented as mean ± SD (n = 3).

The improvements in solubility and dissolution are consistent with the integrated solid-state data. PXRD showed loss of long-range crystallographic order, FTIR supported altered hydrogen-bonding interactions between ATC and NIC, DSC showed disappearance of the NIC melting event without a sharp cocrystal melting endotherm, TGA revealed altered mass-loss behaviour, and SEM showed a change from faceted particles to irregular agglomerates. Together, these results support the formation of a predominantly amorphous or co-amorphous ATC–NIC multicomponent solid with possible residual crystallinity. The improved pharmaceutical performance is therefore plausibly associated with reduced crystallinity, altered intermolecular interactions, and faster ATC release from the transformed solid. Nevertheless, because physical-mixture solubility and dissolution controls were not tested, the enhancement should not be attributed exclusively to co-amorphisation (Indra et al., 2026).

CONCLUSIONS

Solvent evaporation of atorvastatin calcium with nicotinamide produced a transformed multicomponent

solid rather than a simple physical mixture or a well-defined crystalline cocrystal. The integrated PXRD, FTIR, DSC, TGA, and SEM evidence showed a loss of long-range crystallographic order, an altered hydrogen-bonding environment, modified thermal and mass-loss behaviour, and morphological changes, supporting the formation of a predominantly amorphous or co-amorphous ATC–NIC solid with possible residual crystallinity. This transformation was accompanied by higher aqueous solubility and faster dissolution than crystalline ATC in both acidic and phosphate buffer media. The performance enhancement is therefore plausibly associated with reduced crystallinity and ATC–NIC intermolecular interaction, although it should not be attributed exclusively to co-amorphisation because physical-mixture solubility and dissolution controls were not included. Further glass-transition analysis, physical stability testing, and post-dissolution solid-state characterisation are required to verify phase homogeneity and the stability of the aqueous solid form.

Acknowledgements: The authors thank the Faculty of Pharmacy, Universitas Bakti Tunas Husada, for institutional support, and PT Kimia Farma (Bandung, Indonesia) for supplying the study materials.

Authors' Contributions: Indra Indra designed and supervised the study, analysed the data, and prepared the manuscript. Wida Salsabila Diena carried out the laboratory work and contributed to data collection. Ade Yeni Aprillia contributed to experimental work and data organisation. Winda Trisna Wulandari contributed to data interpretation and manuscript review. All authors read and approved the final version of the manuscript.

Competing Interests: The authors declare no competing interests.

Funding: This research received no specific funding.

REFERENCES

Akour, Y. A., Aljaberi, A., Hamed, S., Al-Taher, A., & Migdadi, E. M. (2025). Preparation, characterization and in vitro evaluation of atorvastatin nanosuspensions. PLOS ONE, 20(10), e0335024. doi:https://doi.org/10.1371/journal.pone.0335024

Al-Kazemi, R., Al-Basarah, Y., & Nada, A. (2019). Dissolution enhancement of atorvastatin calcium by cocrystallization. Advanced Pharmaceutical Bulletin, 9(4), 559-570. doi:https://doi.org/10.15171/apb.2019.064

Aljohani, M., Pallipurath, A. R., McArdle, P., & Erxleben, A. (2017). A comprehensive cocrystal screening study of chlorothiazide. Crystal Growth & Design, 17(10), 5223-5232. doi:https://doi.org/10.1021/acs.cgd.7b00745

Dutt, B., Choudhary, M., & Budhwar, V. (2021). Preparation, characterization and evaluation of fenofibrate: Benzoic acid cocrystals with enhanced pharmaceutical properties. Future Journal of Pharmaceutical Sciences, 7(1), 170. doi:https://doi.org/10.1186/s43094-021-00320-5

Emami, S., & Shayanfar, A. (2021). Comments on "Dissolution enhancement of atorvastatin calcium by cocrystallization". Advanced Pharmaceutical Bulletin, 11(3), 578-579. doi:https://doi.org/10.34172/apb.2021.067

Fael, H., & Demirel, A. L. (2020). Tannic acid as a co-former in co-amorphous systems: Enhancing their physical stability, solubility and dissolution behavior. International Journal of Pharmaceutics, 584, 119284. doi:https://doi.org/10.1016/j.ijpharm.2020.119284

Fo'ad, T., Hameed, G. S., & Raauf, A. M. R. (2022). Thermal analysis in the pre-formulation of amorphous solid dispersion for poorly water-soluble drugs. International Journal of Drug Delivery Technology, 12(4), 1595-1599. doi:https://doi.org/10.25258/ijddt.12.4.19

Gadade, D. D., & Pekamwar, S. S. (2016). Pharmaceutical cocrystals: Regulatory and strategic aspects, design and development. Advanced Pharmaceutical Bulletin, 6(4), 479-494. doi:https://doi.org/10.15171/apb.2016.062

Gao, L., & Zhang, X. R. (2020). Synthesis of two novel azilsartan cocrystals: Preparation, physicochemical characterization and solubility studies. Crystals, 10(9), 739. doi:https://doi.org/10.3390/cryst10090739

Ghosh, T., Juturu, T., Nagar, S. N., & Kamath, S. (2021). Cocrystals of modafinil-nicotinic acid: A novel cocrystal for enhanced bioavailability. Proceedings, 62(1), 12. doi:https://doi.org/10.3390/proceedings2020062012

Ghyadh, B. K. K., & Al-Khedairy, E. B. H. (2023). Solubility and dissolution enhancement of atorvastatin calcium using phospholipid solid dispersion technique. Iraqi Journal of Pharmaceutical Sciences, 32(Suppl.), 244-253. doi:https://doi.org/10.31351/vol32issSuppl.pp244-253

Haskins, M. M., & Zaworotko, M. J. (2021). Screening and preparation of cocrystals: A comparative study of mechanochemistry vs slurry methods. Crystal Growth & Design, 21(7), 4141-4150. doi:https://doi.org/10.1021/acs.cgd.1c00418

Indra, I., Nurani, R., & Wulandari, W. T. (2025). Enhanced solubility and dissolution of ketoconazole through co-amorphization with fumaric and tartaric acids via co-milling. Sains Malaysiana, 54(6), 1593-1604. doi:https://doi.org/10.17576/jsm-2025-5406-14

Indra, I., Tika, R. M., & Wulandari, W. T. (2026). Application of quasi-emulsion solvent diffusion for spherical crystallization of atorvastatin with HPMC E50. Biology, Medicine, & Natural Product Chemistry, 15(1), 475-481. doi:https://doi.org/10.14421/biomedich.2026.151.475-481

Indra, I., Wikarsa, S., Nugraha, Y. P., Suendo, V., Uekusa, H., & Soewandhi, S. N. (2023). Utilizing hot-stage polarized microscopy and ATR-FTIR for ramipril co-crystal screening, supported by principal component analysis and cluster analysis. Journal of Pharmacy & Pharmacognosy Research, 11(6), 1137-1148. doi:https://doi.org/10.56499/jppres23.1723_11.6.1137

Karagianni, A., Malamatari, M., & Kachrimanis, K. (2018). Pharmaceutical cocrystals: New solid phase modification approaches for the formulation of APIs. Pharmaceutics, 10(1), 18. doi:https://doi.org/10.3390/pharmaceutics10010018

Kumar, A., Singh, P., & Nanda, A. (2020). Hot stage microscopy and its applications in pharmaceutical characterization.

Applied Microscopy, 50(1), 12. doi:https://doi.org/10.1186/s42649-020-00032-9

Liu, Q., Yang, D., Chen, T., Zhang, B., Xing, C., Zhang, L., Lü, Y., & Du, G. (2021). Insights into the solubility and structural features of four praziquantel cocrystals. Crystal Growth & Design, 21(11), 6321-6331. doi:https://doi.org/10.1021/acs.cgd.1c00785

Ouiyangkul, P., Tantishaiyakul, V., & Hirun, N. (2020). Exploring potential coformers for oxyresveratrol using principal component analysis. International Journal of Pharmaceutics, 587, 119630. doi:https://doi.org/10.1016/j.ijpharm.2020.119630

Saganowska, P., & Wesołowski, M. (2017). Principal component and cluster analyses as supporting tools for co-crystals detection. Journal of Thermal Analysis and Calorimetry, 130(1), 45-55. doi:https://doi.org/10.1007/s10973-017-6436-8

Shayanfar, A., & Jouyban, A. (2014). Physicochemical characterization of a new cocrystal of ketoconazole. Powder Technology, 262, 242-248. doi:https://doi.org/10.1016/j.powtec.2014.04.072

Skotnicki, M., Jadach, B., Skotnicka, A., Milanowski, B., Tajber, L., Pyda, M., & Kujawski, J. (2021). Physicochemical characterization of a co-amorphous atorvastatin-irbesartan system with a potential application in fixed-dose combination therapy. Pharmaceutics, 13(1), 118. doi:https://doi.org/10.3390/pharmaceutics13010118

Song, X., Luo, Y., Zhao, W., Liu, S., Wang, Y., & Zhang, H. (2024). Preparation and characterization of lutein co-amorphous formulation with enhanced solubility and dissolution. Foods, 13(13), 2029. doi:https://doi.org/10.3390/foods13132029

Telange, D. R., Agrawal, S., Pethe, A. M., & Hadke, A. V. (2023). Enhanced aqueous solubility and in vitro dissolution of the anti-hyperlipidemic agent using synthesized solid dispersion carrier. International Journal of Applied Pharmaceutics, 15(1), 121-130. doi:https://doi.org/10.22159/ijap.2023v15i1.46657

Wesołowski, M. (2025). Methods of thermal analysis as fast and reliable tools for identification and quantification of active ingredients in commercially available drug products. Pharmaceutics, 17(9), 1099. doi:https://doi.org/10.3390/pharmaceutics17091099

THIS PAGE INTENTIONALLY LEFT BLANK